Supplemental Material

Construction of piezoelectric photocatalyst Au/$BiVO_4$ for efficient degradation of tetracycline and studied at single-particle level

Yujia Zhang[1], Yan Liu[2], Xueqin Gong[1], Zeyan Wang[1], Yuanyuan Liu[1], Peng Wang[1], Hefeng Cheng[1], Baibiao Huang[1], Zhaoke Zheng[1,*]

[1]State Key Laboratory of Crystal Materials, Shandong University, Jinan 250100, Shandong, China.
[2]Center for Optics Research and Engineering, Shandong University, Qingdao 266237, Shandong, China.

[*]**Correspondence to:** Prof. Zhaoke Zheng, State Key Laboratory of Crystal Materials, Shandong University, 27 Shanda South Road, 250100, China. E-mail: zkzheng@sdu.edu.cn

EXPERIMENTAL MATERIALS AND METHODS

Deposition of single metals/oxides on monoclinic $BiVO_4$

For the facet-selective photo depositions, two ways containing single reduction and single oxidation were carried out at room temperature without pH value adjusted. Normally, 0.2 g m-$BiVO_4$ powder and a calculated amount of metal precursors (3 wt. %) were mixed in 100 mL deionized water. The suspension was then irradiated by a 300 W Xe lamp ($\lambda > 420$ nm) under continuous stirring. After 5 h photo-deposition, the suspension was filtered, washed with deionized water for more than three times, and finally dried at 60 °C for overnight.

Characterizations

The X-ray diffraction (XRD) spectra of the obtained products were recorded on a Bruker D8 Advance X-ray diffractometer with Cu Kα irradiation. Scanning electron microscope (SEM) was performed on a Hitachi S-4800 scanning electron microscope to obtain the surface morphologies and detailed nanostructure. Transmission electron microscope (TEM) was performed on a JEOL-2011 transmission electron microscope (Japan) at 200 kV to

characterize the morphology and microstructures. X-ray photoelectron spectroscopy (XPS) was characterized by Thermo Fisher Scientific Escalab 250 spectrometer to research the surface chemical compositions and states of samples, and the binding energies was calibrated by C 1s peak at 284.6 eV. The Raman measurement was performed on the Nanophoton Raman-11 system equipped with an upright microscope (Nikon Eclipse 90i) and a 600 grooves/mm grating. 633 nm laser was used for all measurements. UV-vis diffuse reflectance spectra (DRS) were recorded using a Shimadzu UV-2600i recording spectrophotometer and equipped with an integrating sphere using $BaSO_4$ as reference. The concentration of the pollutant was determined with a UV-vis spectrophotometer on TU-1810PC.

Photoelectrocatalytic measurements

Electrochemical impedance spectra (EIS) were measured under dark at 0.58 V *vs*. Ag/Ag^+ in the frequency range of $0.1\text{-}10^5$ Hz with an AC voltage amplitude of 10 mV. The transient open-circuit voltage decay experiments were taken for 350 s. Mott-Schottky measurements were recorded at a frequency of 1k Hz. The *in situ* impedance spectrum of the samples was carried out by an electrochemical analyzer (Ivium Stat, Netherlands).

Supplementary Figures

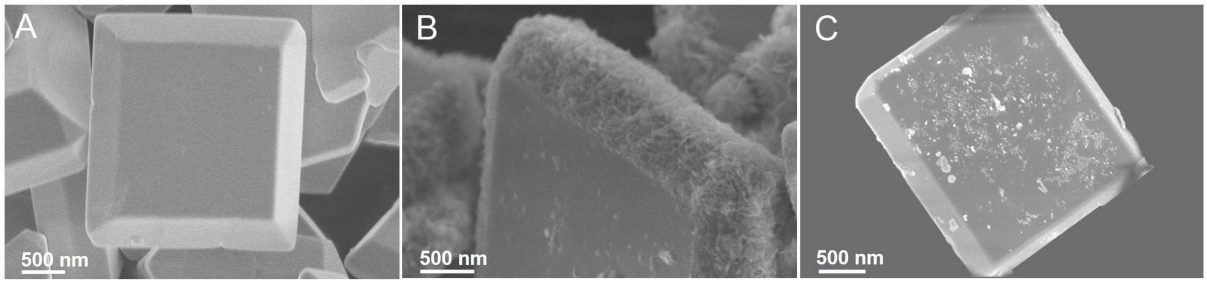

Supplementary Figure 1. SEM images of $BiVO_4$ and with single metal/oxide deposited. (A) $BiVO_4$; (B) $MnO_2/BiVO_4$; (C) $Pt/BiVO_4$.

As shown in Supplementary Figure 1, the reduction (Pt) and oxidation (MnO_2) catalysts were selectively photo-deposited on the (010) and (110) facets.

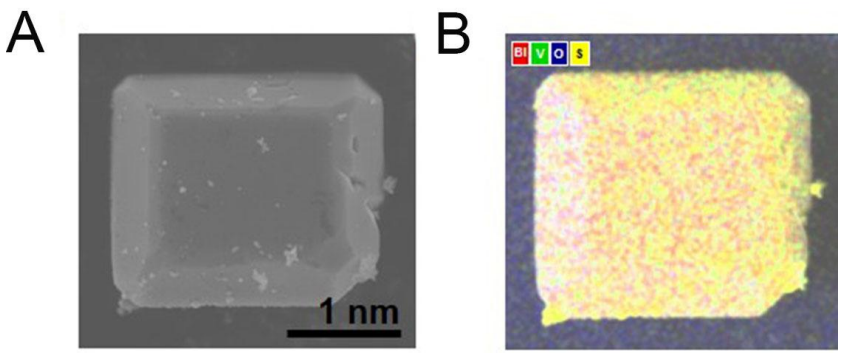

Supplementary Figure 2. (A) STEM of $3Au/BiVO_4$; (B) EDS elemental mapping images of the $3Au/BiVO_4$ sample.

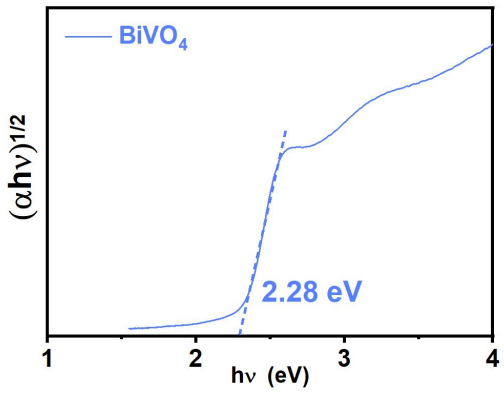

Supplementary Figure 3. Corresponding Kubelka-Munk transformed reflectance spectra of $BiVO_4$.

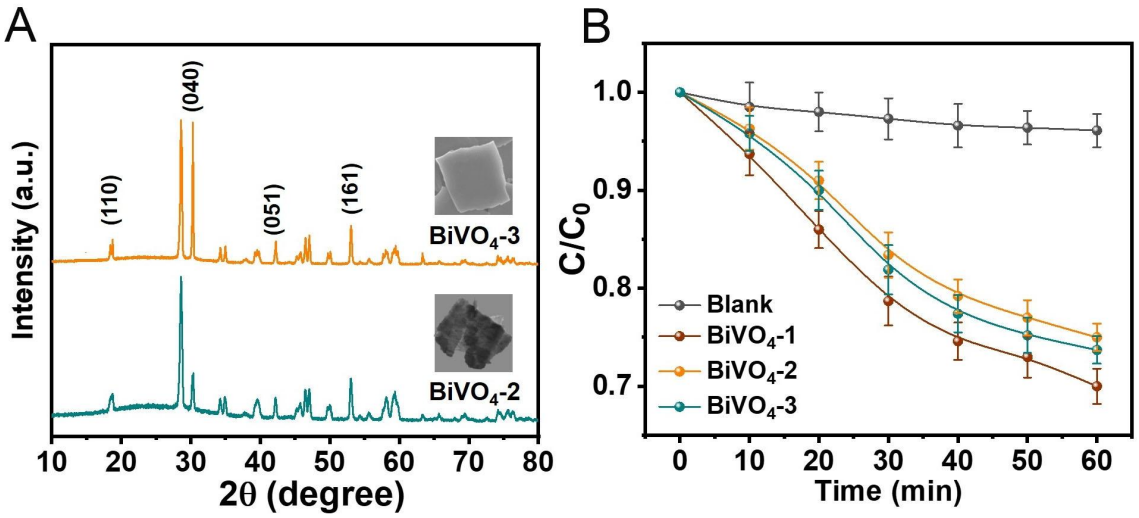

Supplementary Figure 4. (A) XRD patterns of $BiVO_4$ with exposed (010) or (110) facets (Inset is the SEM images); (B) Catalytic degradation performance of TC under ultrasonic stimulation.

The experimental details are shown in EXPERIMENTAL MATERIALS AND METHODS. Supplementary Figure 4a presents X-ray diffractometer (XRD) patterns of $BiVO_4$ samples. Herin, the co-exposed (010) and (110) facets are named $BiVO_4$-1, the exposed (010) facets are named $BiVO_4$-2, and the exposed (110) facets are named $BiVO_4$-3. As shown in Supplementary Figure 4B, the decahedral $BiVO_4$ with co-exposed two facets exhibits the optimal piezoelectric catalytic performance.

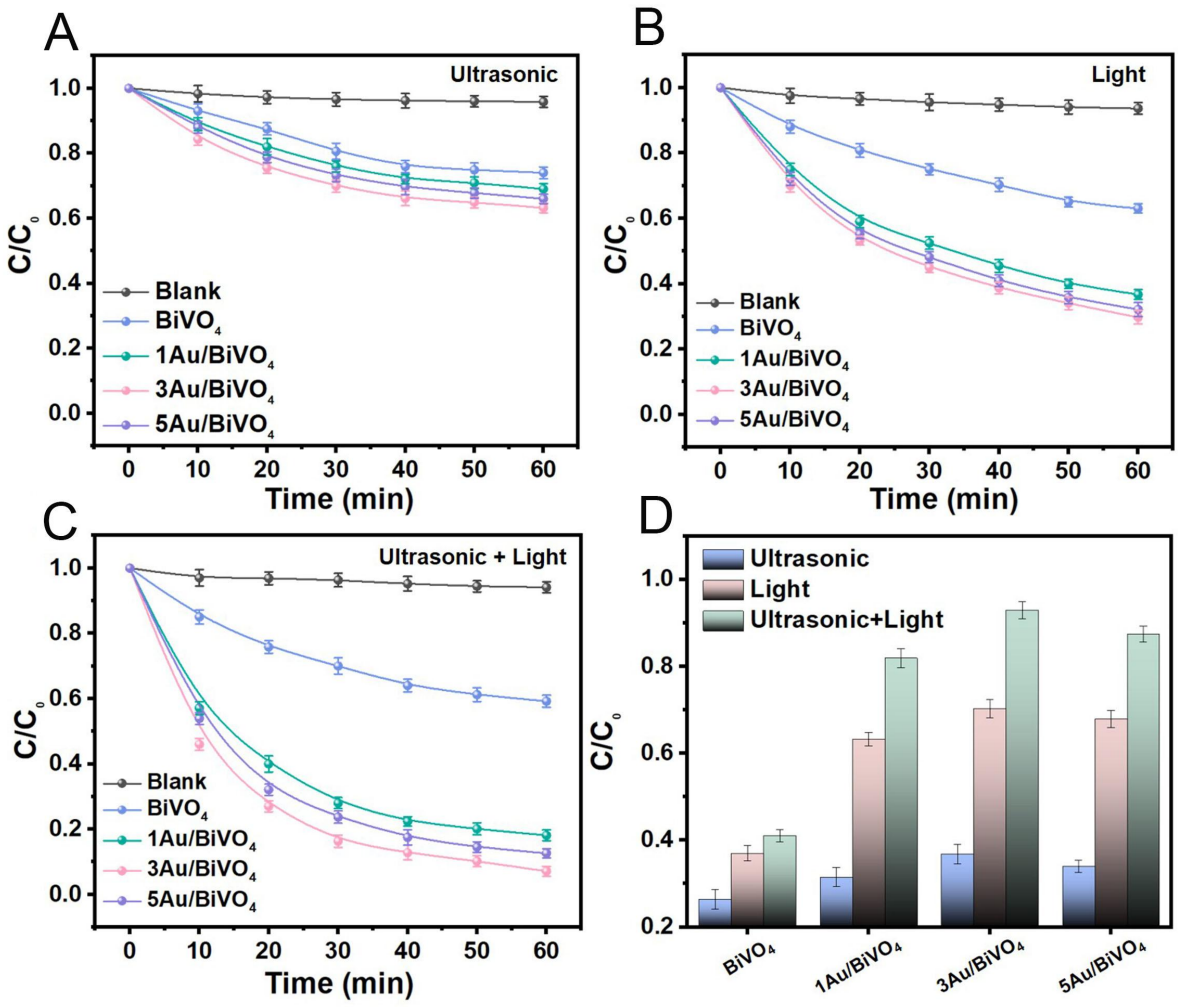

Supplementary Figure 5. Catalytic degradation performance of RhB over different samples. (A) Under ultrasonic stimulation; (B) Under visible light irradiation; (C) Catalysis test simultaneous ultrasonic and light irradiation; (D) Comparison of the ultrasonic, photocatalytic, and both ultrasonic and light irradiation degradation of RhB over samples for 60 min.

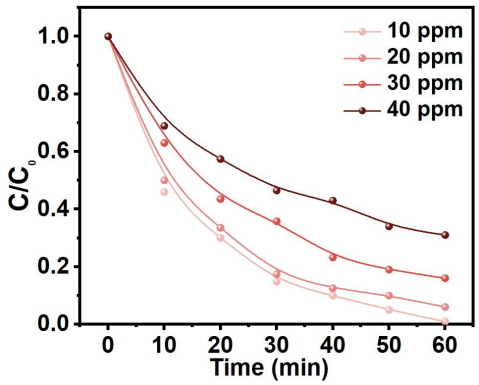

Supplementary Figure 6. Piezoelectric photocatalytic activity of 3Au/$BiVO_4$ at different TC concentrations.

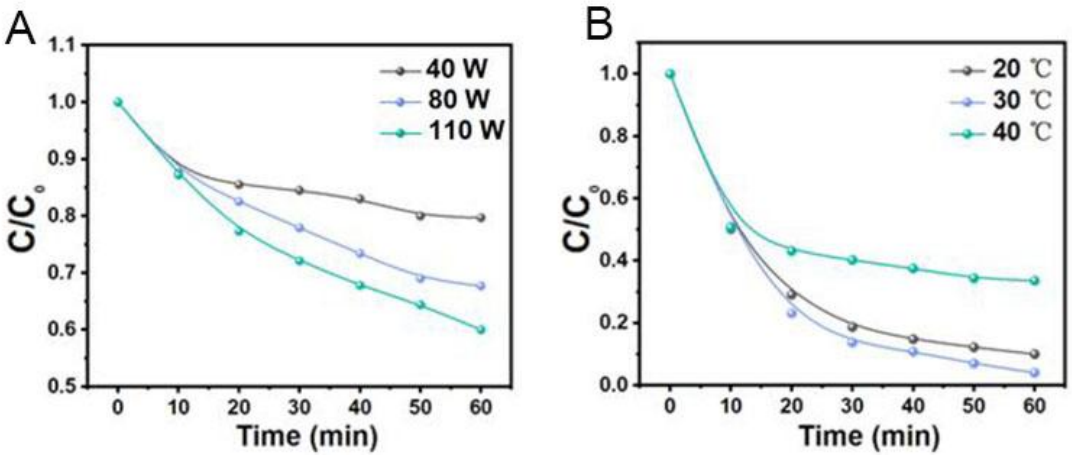

Supplementary Figure 7. The removal of 4-CP by 3Au/$BiVO_4$ with different (A) ultrasonic power and (B) temperature.

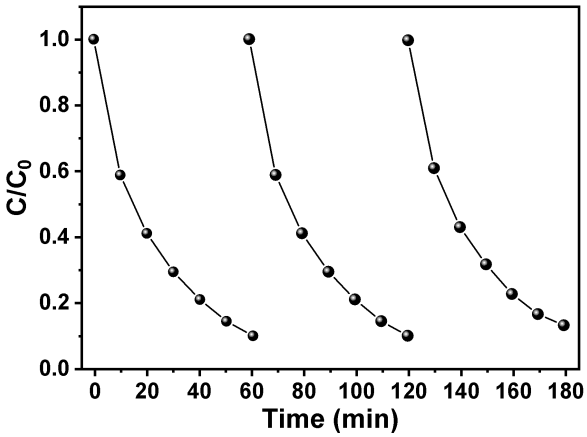

Supplementary Figure 8. Three cycle runs toward pizo-photocatalytic of TC over 3Au/$BiVO_4$.

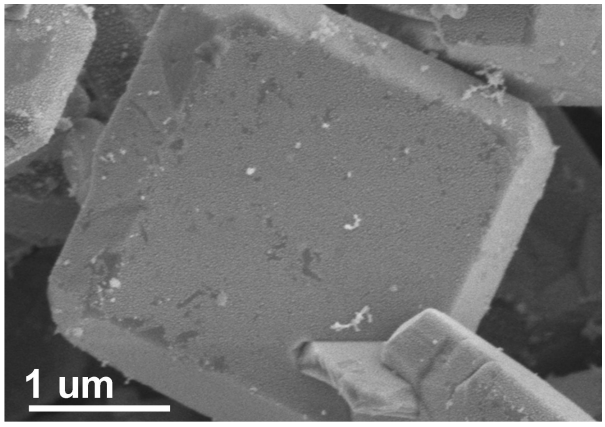

Supplementary Figure 9. SEM image of 3Au/$BiVO_4$ after photodegradation of TC.

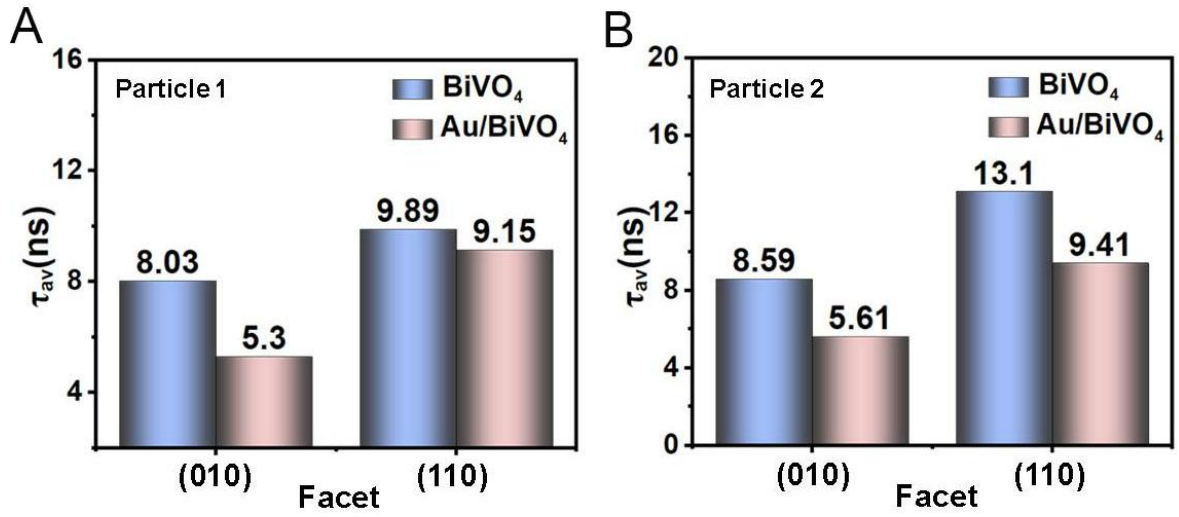

Supplementary Figure 10. (A and B)The intensity-weighted average lifetimes (τ_{av}) observed of different facets on different particles of $BiVO_4$ and 3Au/$BiVO_4$.

We select two single particles of $BiVO_4$ and 3Au/$BiVO_4$ for testing, named “Particle 1” and “Particle 2”, respectively. The results show that the PL lifetime of 3Au/$BiVO_4$ is shortened relative to that of $BiVO_4$, regardless of the representative site or facets.

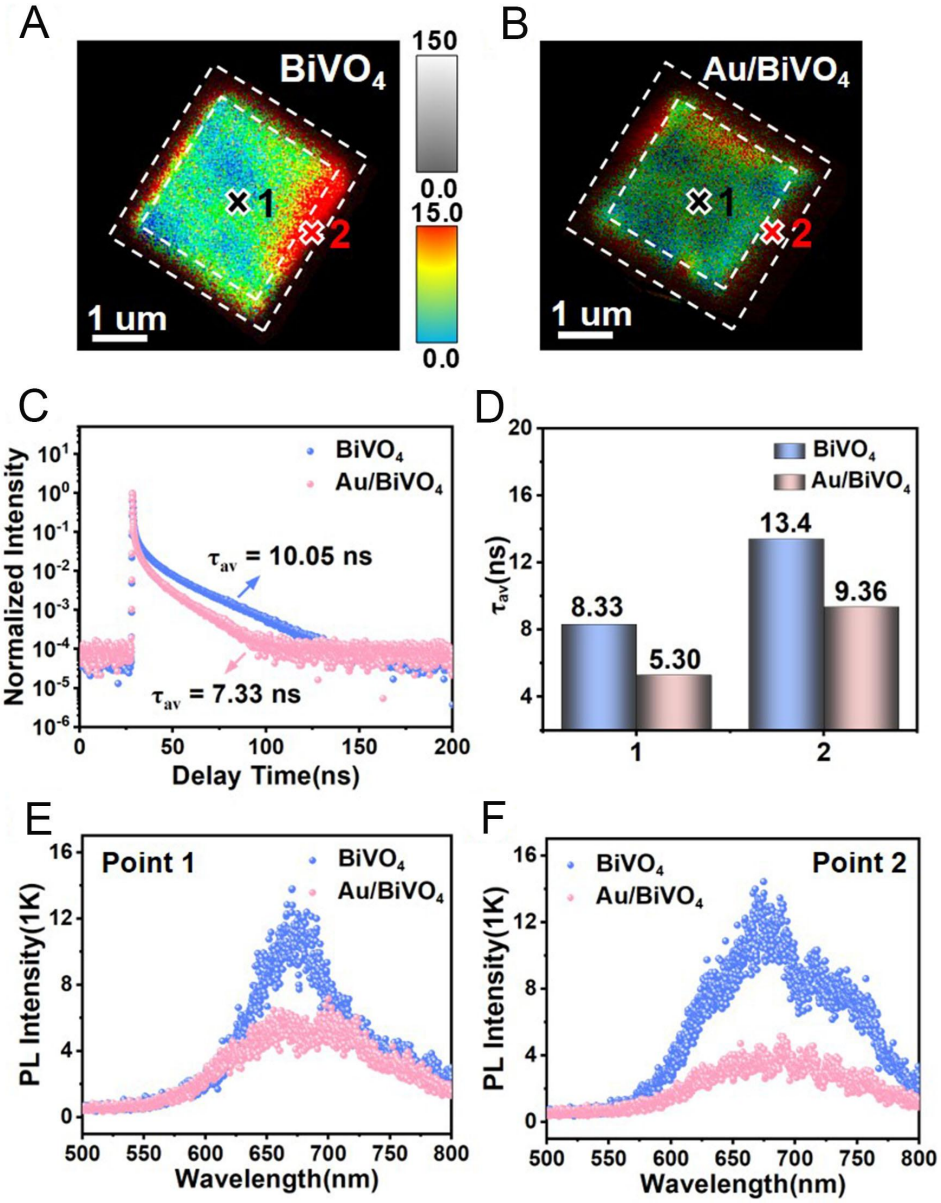

Supplementary Figure 11. Single-particle PL spectroscopy measurements. PL lifetime mapping of (A) another single $BiVO_4$ particleand (B) another single 3Au/$BiVO_4$ particle; (C) Time-resolved photoluminescence (TRPL) spectra of entire $BiVO_4$ and 3Au/$BiVO_4$ particle; (D) The intensity-weighted average lifetimes (τ_{av}) observed of representative sites (Point 1 and Point 2) on single $BiVO_4$ and 3Au/$BiVO_4$ particle; (E and F) The corresponding PL emission spectra were observed at representative sites on single $BiVO_4$ and 3Au/$BiVO_4$ particle.

Supplementary Figure 11 shows the single-particle spectroscopy tests of the other two $BiVO_4$ and 3Au/$BiVO_4$ particles. Supplementary Figure 11A and B shows the PL lifetime mapping of $BiVO_4$ and 3Au/$BiVO_4$ particles. Supplementary Figure 11C and D indicate that both the overall particle and representative sites exhibit a significantly shorter PL lifetime of 3Au/$BiVO_4$ (7.33 ns) compared to $BiVO_4$ (10.05 ns). Meanwhile, PL spectra testing also confirmed that the emission intensity of 3Au/$BiVO_4$ is lower than that of $BiVO_4$, which is consistent with our previous conclusion [Supplementary Figure 11E and F].

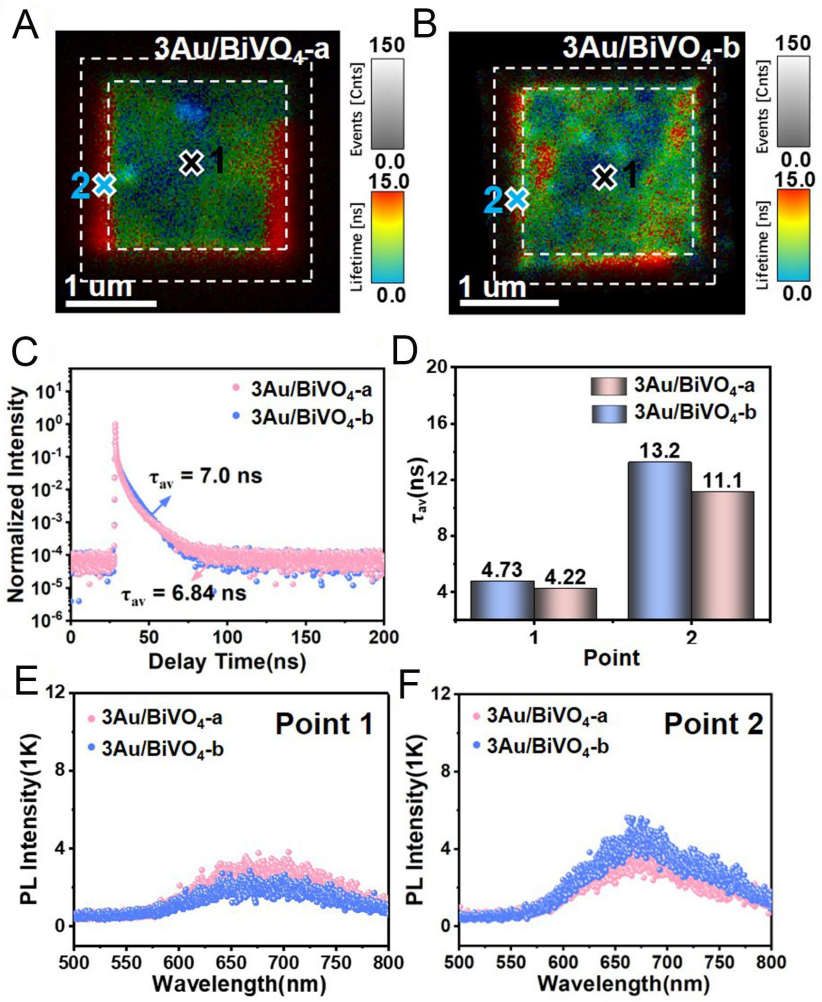

Supplementary Figure 12. Single-particle PL spectroscopy measurements. PL lifetime mapping of (A) a single 3Au/$BiVO_4$ particle; (B) another 3Au/$BiVO_4$ particle; (C) Time-resolved photoluminescence (TRPL) spectra of entire 3Au/$BiVO_4$ particles; (D) The intensity-weighted average lifetimes (τ_{av}) observed of representative sites (Point 1 and Point 2) on different particles of 3Au/$BiVO_4$; (E and F) The corresponding PL emission spectra were observed at representative sites on different particles of 3Au/$BiVO_4$.

To verify our conclusion, we selected two 3Au/$BiVO_4$ particles for single-particle spectral testing, and the test results are shown in Supplementary Figure 12. Supplementary Figure 12A and B represent the PL mapping of two particles, respectively. The overall PL lifetime of the two particles is 7.0 and 6.84 ns respectively, which is shorter compared to $BiVO_4$ and consistent with the conclusion we draw in the paper [Supplementary Figure 12C]. In fact, it is impossible to guarantee that all crystals are uniform that obtained by chemical synthesis. The process of nucleation, growth and recrystallization are not completely consistent, which leads to certain differences between particles. This difference is bound to affect the lifetime of particles. Because the difference between particles is inevitable, it is necessary to study the single-particle spectrum. Compared with the traditional measurements obtained by ensemble averaging, the single particle study can more accurately reflect the changes in spatial resolution caused by heterostructures.

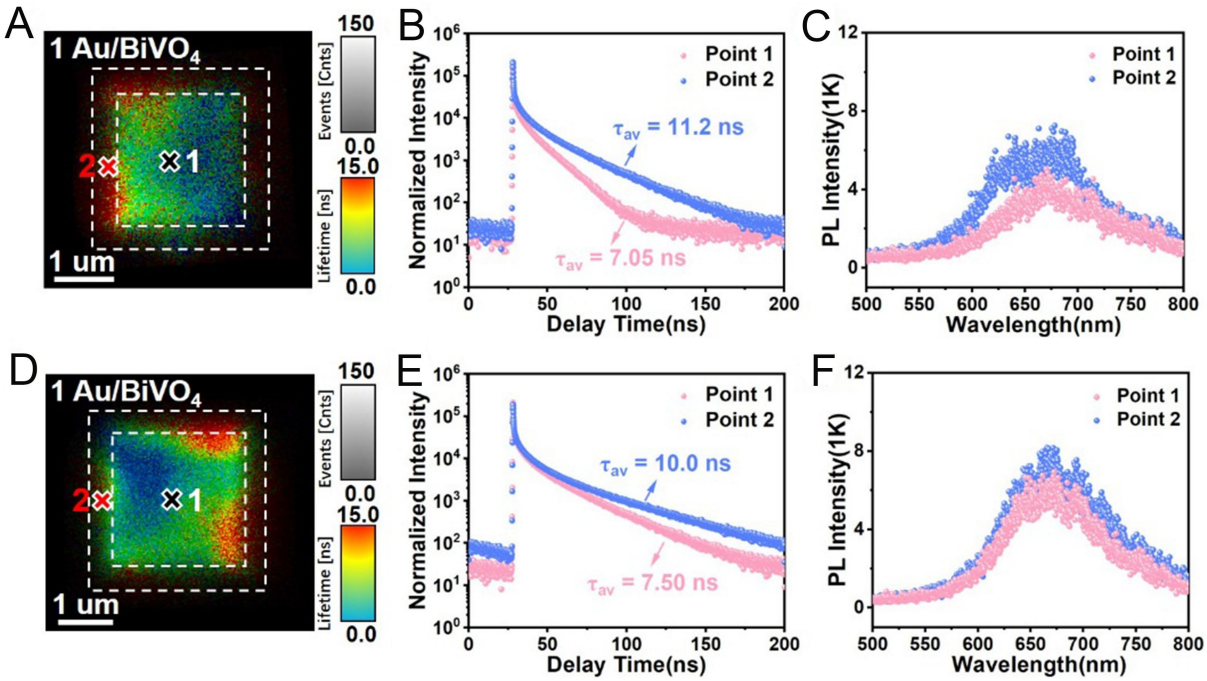

Supplementary Figure 13. (A) PL lifetime mapping of 1Au/$BiVO_4$; (B) TPRL spectra of representative sites (Point 1 and Point 2) on 1Au/$BiVO_4$; (C) PL intensity of representative sites; (D) PL lifetime mapping of another 1Au/$BiVO_4$ particle; (E) TPRL spectra of representative sites (Point 1 and Point 2) on another 1Au/$BiVO_4$ particle; (F) PL intensity of representative sites on another 1Au/$BiVO_4$ particle.

By comparing the single-particle spectra of $BiVO_4$, 1Au/$BiVO_4$ and 3Au/$BiVO_4$, it can be concluded that although the PL lifetime of 1Au/$BiVO_4$ particles is shorter than that of $BiVO_4$, it is still longer than that of 3Au/$BiVO_4$, indicating limited hot electron injection effects in 1Au/$BiVO_4$.

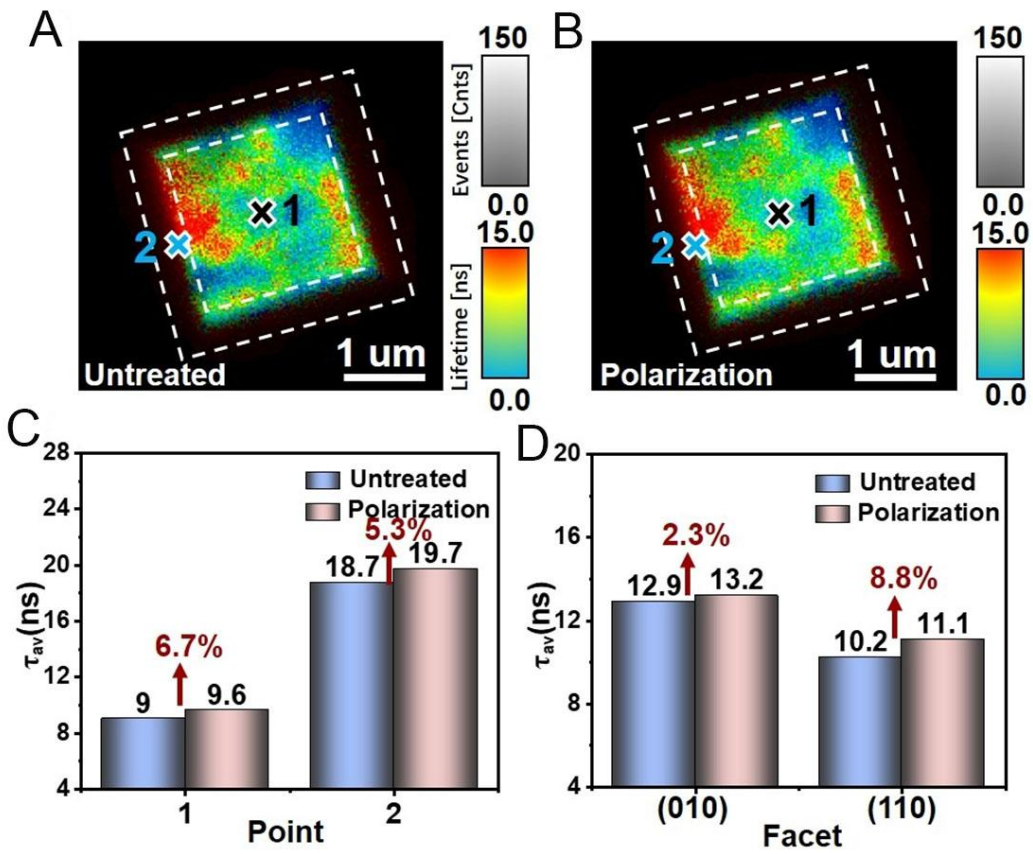

Supplementary Figure 14. *In situ* single-particle PL spectroscopy measurements. PL lifetime mapping of a single $BiVO_4$ particle (A) before and (B) after polarization treatment. (C) The τ_{av} observed of representative sites with τ_{av} increase rate for $BiVO_4$ particle before and after polarization treatment; (D) The τ_{av} observed of different facets with τ_{av} increase rate for $BiVO_4$ particle before and after polarization treatment.

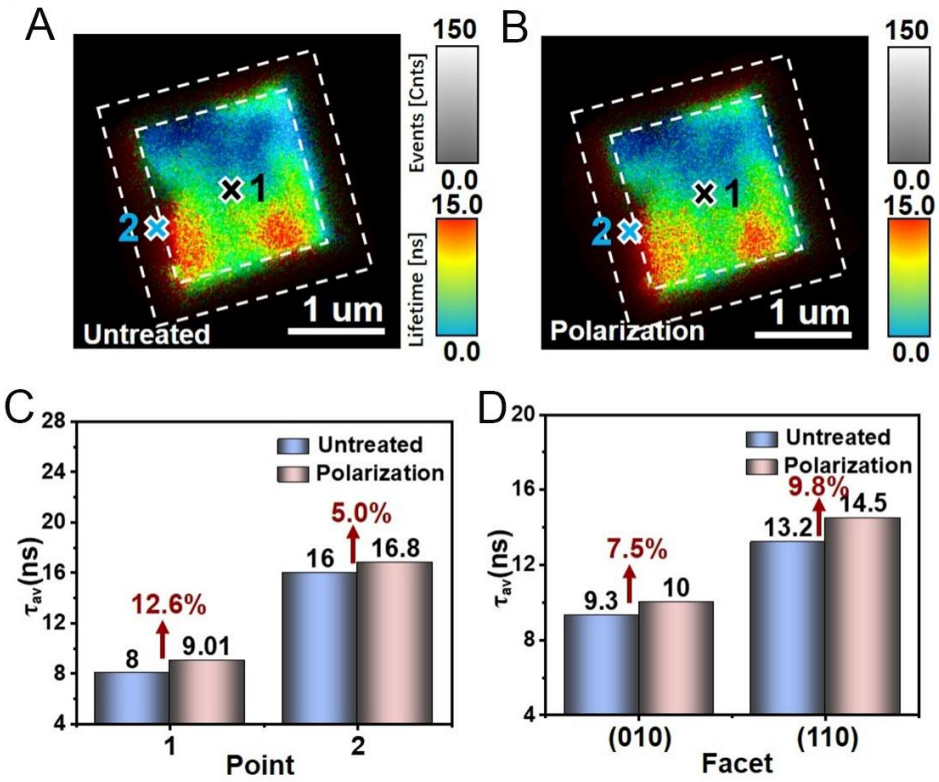

Supplementary Figure 15. *In situ* single-particle PL spectroscopy measurements. PL lifetime mapping of another $BiVO_4$ particle (A) before and (B) after polarization treatment; (C) The τ_{av} observed of representative sites with τ_{av} increase rate for another $BiVO_4$ particle before and after polarization treatment; (D) The τ_{av} observed of different facets with τ_{av} increase rate for another $BiVO_4$ particle before and after polarization treatment.

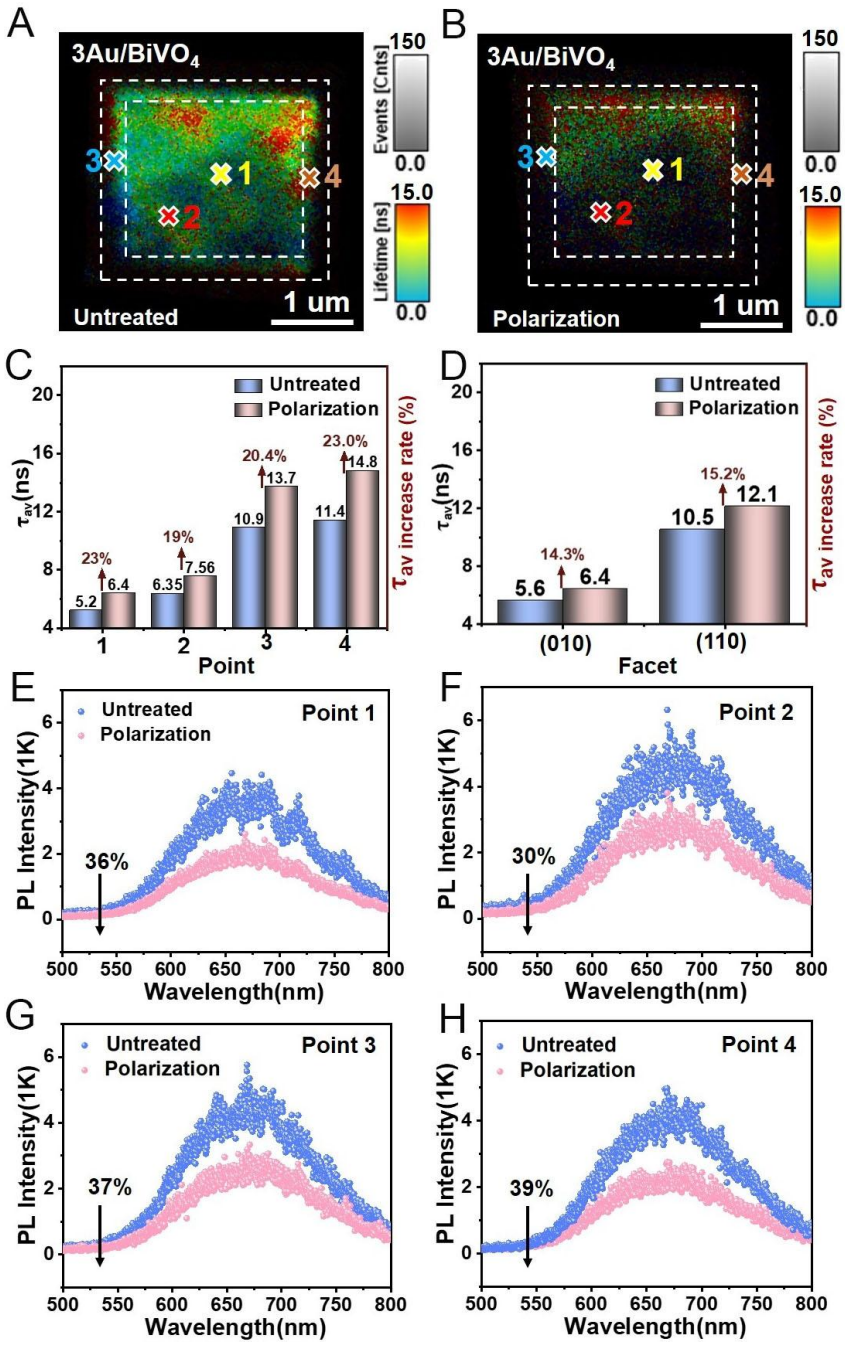

Supplementary Figure 16. *In situ* single-particle PL spectroscopy measurements. PL lifetime mapping of a single 3Au/$BiVO_4$ particle (A) before and (B) after polarization treatment; (C) The τ_{av} observed of representative sites with τ_{av} increase rate before and after polarization treatment; (D) The τ_{av} observed of different facets with τ_{av} increase rate before and after polarization treatment; (E-H) The PL emission intensity of representative sites with decay rate before and after polarization treatment.

We simulate the promoting effect of piezoelectric potential on charge separation by

polarizing different particles. After in-situ polarization treatment of 3Au/$BiVO_4$, as shown in Supplementary Figure 16B and C, the PL lifetime increase rates of different sites were 23%, 19%, 20.4%, and 23%, respectively. Fitting the two crystal planes showed lifetime increase rates of 14.3% and 15.2%, respectively. This result indicates that the PL lifetime increase rates of 3Au/$BiVO_4$ is greater than that of $BiVO_4$. This may be due to the piezoelectric polarization charge generated by $BiVO_4$ crystals under ultrasound being transferred to Au to drive catalytic reactions.

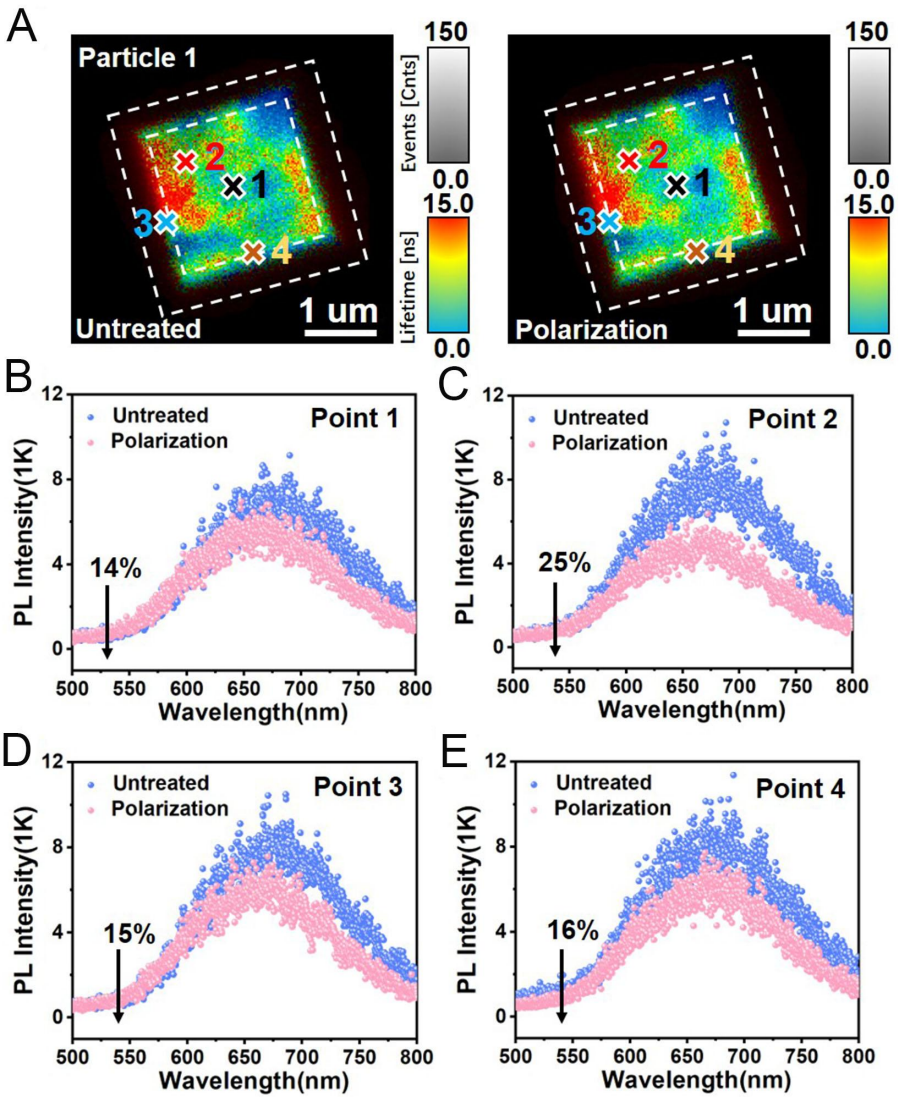

Supplementary Figure 17. *In situ* single-particle PL spectroscopy measurements. (A) PL lifetime mapping of a single $BiVO_4$ particle before and after polarization treatment; (B-E) The PL emission intensity of representative sites with decay rate before and after polarization treatment.

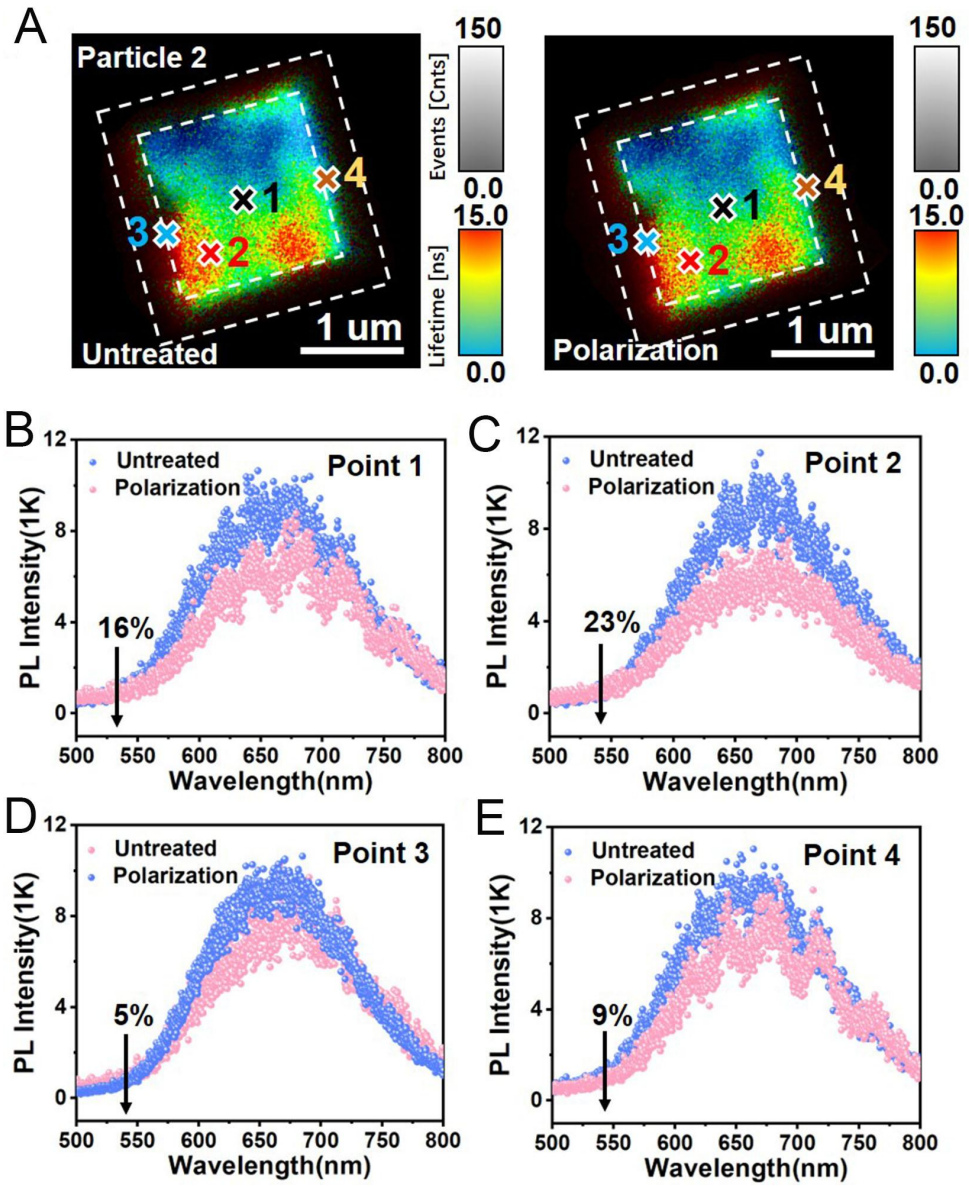

Supplementary Figure 18. *In situ* single-particle PL spectroscopy measurements. (A) PL lifetime mapping of another single $BiVO_4$ particle before and after polarization treatment. (B-E) The PL emission intensity of representative sites before and after polarization treatment.

We have chosen another $BiVO_4$ particle for in-situ polarization treatment to better validate our conclusion. As shown in Supplementary Figure 18C and D, the PL intensity decay rate of $BiVO_4$ at different sites is less than $3Au/BiVO_4$, indicating that AuNPs promote charge separation.

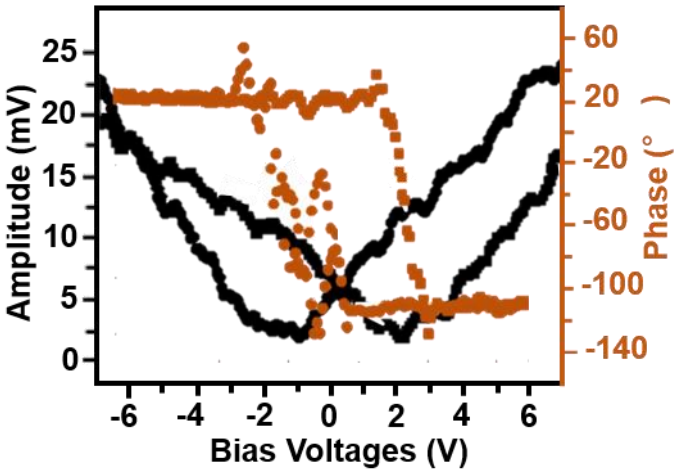

Supplementary Figure 19. The phase hysteresis loop and amplitude butterfly loop for 3Au/$BiVO_4$.

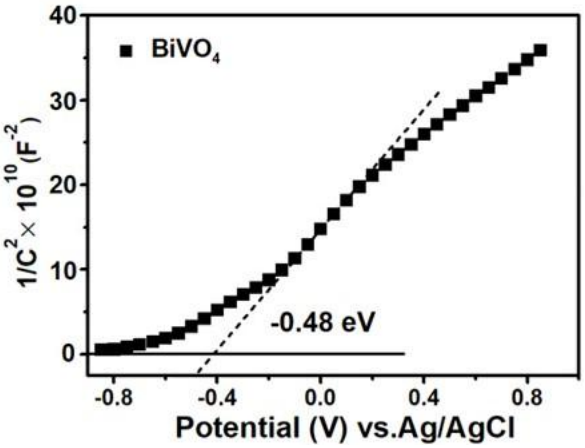

Supplementary Figure 20. M-S plot of $BiVO_4$.

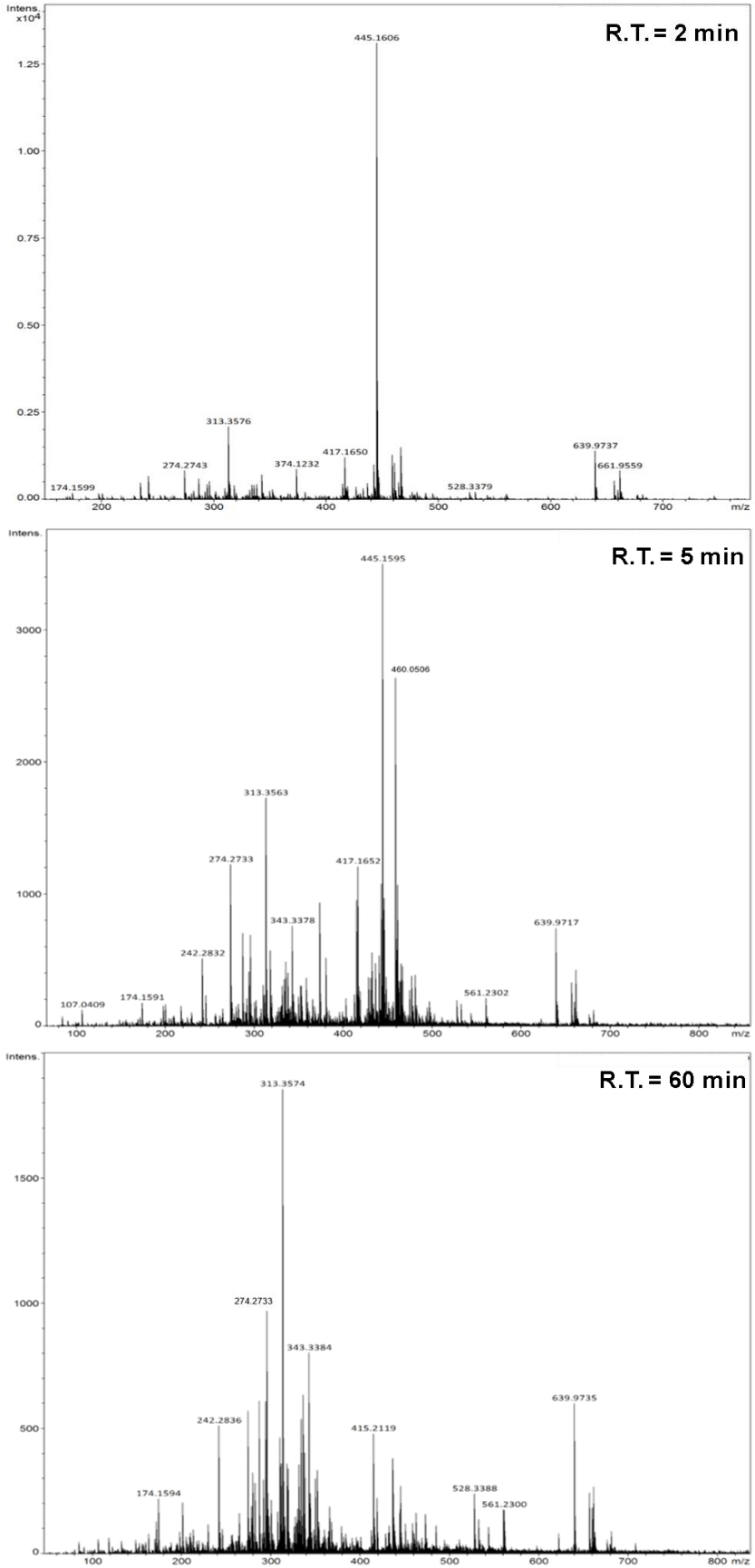

Supplementary Figure 21. Mass spectra of TC degradation intermediates at different times (R.T. = reaction time).

Supplementary Tables

Supplementary Table 1. Comparison of photocatalytic performance between 3Au/$BiVO_4$ and other photocatalysts reported in recent years

Materials	Catalyst (mg/L)	TC/RhB (mg/L)	Time (min)	Reduction rate (%)	Ref.
Au/$BiVO_4$	0.4	20	60	95.0	This work
Ag/Ag_2CO_3/$BiVO_4$	0.4	20	150	94.9	Liu *et al*., (2018)[1]
$In_{2.77}S_4$/$BiVO_4$	0.5	10	90	89.9	Wu *et al*., (2022)[2]
V-$BiOIO_3$/FTCN	0.2	10	60	89.0	Wu *et al*., (2023)[3]
LDH–EDTA–Zn	400 mm^2	20	25	99.7	Ali khan *et al*., (2024)[4]
$BaTiO_3$/tubular g-C_3N_4	0.4	10	60	91.0	Gong *et al*., (2023)[5]
Fe-based MOFs	0.5	50	180	96.6	Wang *et al*., (2018)[6]
$CuInS_2$/Bi_2MoO_6	0.6	20	120	84.7	Guo *et al*., (2021)[7]
$Na_{0.5}Bi_{0.5}TiO_3$	1	10	100	99	Ji *et al*., (2022)[8]
AN-TCN	1	10	30	86.0	Wu *et al*., 2022[9]
TiO_2/Fe_3O_4/BC	0.35	10	45	83	Asgharzadeh *et al*., (2021)[10]

Supplementary Table 2. Kinetic Parameters of the TPRL Lifetimes for $BiVO_4$ (τ)[a]

Samples	τ_1 (ns)	τ_2 (ns)	τ_3 (ns)	A_1[b]	A_2[b]	A_3[b]
Particle 1	0.45 ± 0.06	2.53 ± 0.20	11.3 ± 0.20	4.77 ± 0.10	6.21 ± 0.10	7.23 ± 0.04
Particle 2	0.53 ± 0.07	2.56 ± 0.15	11.9 ± 0.10	4.83 ± 0.04	6.30 ± 0.10	7.26 ± 0.20

[a]Kinetic Parameters of the TPRL Lifetimes over entire $BiVO_4$ single-particles. The multiexponential decay curves were fitted using a nonlinear least-squares method with a multicomponent decay law given by:

$$I(\mathrm{t}) = A_1 \exp(-t/\tau_1) + A_2 \exp(-t/\tau_2) + \ldots + A_i \exp(-t/\tau_i);$$

[b]Coefficient value of the fitting.

Supplementary Table 3. Kinetic Parameters of the TPRL Lifetimes for $BiVO_4$ (τ)[a]

Samples	Points	τ_1 (ns)	τ_2 (ns)	τ_3 (ns)	A_1	A_2	A_3
Particle 1	1	0.26 ± 0.03	1.65 ± 0.06	8.89 ± 0.02	3.89 ± 0.03	6.50 ± 0.06	7.00 ± 0.05
	2	0.34 ± 0.02	2.20 ± 0.05	10.8 ± 0.02	4.40 ± 0.14	6.89 ± 0.14	8.39 ± 0.04
Particle 2	1	0.30 ± 0.07	1.93 ± 0.20	9.41± 0.20	4.09 ± 0.06	6.68 ± 0.20	7.26 ± 0.20
	2	0.44 ± 0.03	2.59 ± 0.10	16.2 ± 0.02	9.00 ± 0.31	9.94 ± 0.13	10.1 ± 0.05

[a]Kinetic Parameters of the TPRL Lifetimes of different points over $BiVO_4$ single-particles.

Supplementary Table 4. Kinetic Parameters of the TPRL Lifetimes for 3Au/$BiVO_4$ (τ)[a]

Samples	τ_1 (ns)	τ_2 (ns)	τ_3 (ns)	A_1[b]	A_2[b]	A_3[b]
Particle 1	0.26 ± 0.06	2.40 ± 0.20	8.86 ± 0.20	4.33 ± 0.10	5.89 ± 0.10	6.03 ± 0.04
Particle 2	0.28 ± 0.06	2.37 ± 0.20	8.69 ± 0.20	4.30 ± 0.10	5.79 ± 0.10	5.88 ± 0.04

[a]Kinetic Parameters of the TPRL Lifetimes over entire 3Au/$BiVO_4$ single-particles.

Supplementary Table 5. Kinetic Parameters of the TPRL Lifetimes for 3Au/$BiVO_4$ (τ)[a]

Samples	Points	τ_1 (ns)	τ_2 (ns)	τ_3 (ns)	A_1	A_2	A_3
Particle 1	1	0.24 ± 0.03	2.02 ± 0.06	6.04 ± 0.02	3.87 ± 0.03	6.41 ± 0.06	6.99 ± 0.05
	2	0.30 ± 0.02	2.21 ± 0.05	9.84 ± 0.02	4.33 ± 0.14	6.77 ± 0.14	8.10 ± 0.04
Particle 2	1	0.29 ± 0.07	2.32± 0.20	6.27± 0.20	4.09 ± 0.06	6.65 ± 0.20	7.47 ± 0.20
	2	0.32 ± 0.03	2.05 ± 0.10	9.58 ± 0.02	4.14 ± 0.31	6.78 ± 0.13	7.34 ± 0.05

[a]Kinetic Parameters of the TPRL Lifetimes of different points over 3Au/$BiVO_4$ single-particles.

The parameters for Particle 1 and Particle 2 here correspond to the particles in Figure 4 and Supplementary Figure 10.

References

[1] Liu, Y., Kong, J. J., Yuan, J. L., Zhao, W., Zhu, X., Sun, C., Xie, J. M., 2018. Enhanced photocatalytic activity over flower-like sphere Ag/Ag_2CO_3/$BiVO_4$ plasmonic heterojunction photocatalyst for tetracycline degradation. Chem. Eng. J. 331, 242-254. https://doi.org/10.1016/j.cej.2017.08.114.

[2] Wu, X.-F., Chang, T. L., Fu, Y. X., Shi, Y. M., Su, J. Z., Wang, Z. H., Ma, X. Y., Wang, H.,2022. Preparation, properties, and photocatalytic mechanism of $In_{2.77}S_4$/$BiVO_4$ heterostructure for tetracycline degradation, J. Mater. Sci.-Mater. Electron. 33, 14680-14690. https://doi.org/10.1007/s10854-022-08387-3.

[3] Wu, T., Liang, Q. H., Tang, L., Tang, J. L., Wang, J. J., Shao, B. B., Gong, S. X., He, Q. Y., Pan, Y., Liu, Z. F., 2023. Construction of a novel S-scheme heterojunction piezoelectric photocatalyst V-$BiOIO_3$/FTCN and immobilization with floatability for tetracycline degradation. J. Hazard. Mater. 443, 130251. https://doi.org/10.1016/j.jhazmat.2022.130251.

[4] Ali khan, M., Safira, A. R., Kaseem, M., 2024. Modulating chelation with pH sensitivity for controlled structural defects and enhanced electrochemical and photocatalytic activities of LDH films. J. Mater. Chem. A. 12, 3411-3433. https://doi.org/10.1039/D3TA06840D.

[5] Gong, S. X., Zhang, W. X., Liang, Z. R., Zhang, Y. J., Gan, T., Hu, Y. U., Huang, Z. Q., 2023. Construction of a $BaTiO_3$/tubular g-C_3N_4 dual piezoelectric photocatalyst with enhanced carrier separation for efficient degradation of tetracycline. Chem. Eng. J. 461, 141947. https://doi.org/10.1016/j.cej.2023.141947.

[6] Wang, D. B., Jia, F. Y., Wang, H., Chen, F., Fang, Y., Dong, W. B., Zeng, G. M., Li, X. M., Yang, Q., Yuan, X. Z., 2018. Simultaneously efficient adsorption and photocatalytic degradation of tetracycline by Fe-based MOFs. J. Colloid Interface Sci. 519, 273-284. https://doi.org/10.1016/j.jcis.2018.02.067.

[7] Guo, J., Wang, L., Wei, X., Alothman, Z. A., Albaqami, M. D., Malgras, V., Yamauchi, Y., Kang, Y., Wang, M., Guan, W., Xu, X., 2021. Direct Z-scheme $CuInS_2$/Bi_2MoO_6 heterostructure for enhanced photocatalytic degradation of tetracycline under visible light. J. Hazard. Mater. 415, 125591. https://doi.org/10.1016/j.jhazmat.2021.125591.

[8] Ji, J., Pu, Y., Ouyang, T., Chang, L., Zhou, S., Zhang, L., 2022. Improving charge separation efficiency and piezo-photodegradation properties in $Na_{0.5}Bi_{0.5}TiO_3$ via lattice

engineering. Ceram. Int. 48, 28629-28639. https://doi.org/10.1016/j.ceramint.2022.06.177.

[9] Wu, T., Liu, Z., Shao, B., Liang, Q., He, Q., Pan, Y., Zhang, X., Liu, Y., Sun, J., Gong, S., 2022. Hydrogen peroxide-impregnated supramolecular precursors synthesize mesoporous-rich ant nest-like filled tubular g-C_3N_4 for effective photocatalytic removal of pollutants. Chem. Eng. J. 447, 137332. https://doi.org/10.1016/j.cej.2022.137332.

[10] Asgharzadeh, F., Kalantary, R. R., Gholami, M., Jafari, A. J., Kermani, M., Asgharnia, H., 2021. TiO_2-decorated magnetic biochar mediated heterogeneous photocatalytic degradation of tetracycline and evaluation of antibacterial activity. Biomass Convers. Biorefinery. 13, 8949-8959. https://doi.org/10.1007/s13399-021-01685-6.